Technical Note

1978-27

R. Weber

The Passive, Ground-Based, Electro-Optical Detection of Synchronous Satellites

19 June 1978

Prepared for the Department of the Air Force
under Electronic Systems Division Contract F19628-78-C-0002 by

Lincoln Laboratory
MASSACHUSETTS INSTITUTE OF TECHNOLOGY
LEXINGTON, MASSACHUSETTS

The work reported in this document was performed at Lincoln Laboratory, a center for research operated by Massachusetts Institute of Technology, with the support of the Department of the Air Force under Contract F19628-78-C-0002.

This technical report has been reviewed and is approved for publication.

FOR THE COMMANDER

Raymond L. Loiselle, Lt. Col., USAF
Chief, ESD Lincoln Laboratory Project Office

MASSACHUSETTS INSTITUTE OF TECHNOLOGY

LINCOLN LABORATORY

THE PASSIVE, GROUND-BASED, ELECTRO-OPTICAL DETECTION OF SYNCHRONOUS SATELLITES

R. WEBER

Group 94

TECHNICAL NOTE 1978-27

19 JUNE 1978

LEXINGTON MASSACHUSETTS

ABSTRACT

M.I.T. Lincoln Laboratory is engaged in supporting the Electronic Systems Division (ESD) of the Air Force Systems Command (AFSC) in developing the Ground-based Electro-Optical Deep Space Surveillance (GEODSS) system. As a part of this program an Experimental Test Site (ETS) has been established in the White Sands Missile Range, New Mexico, to serve as a test-bed for the system. After a brief description of the GEODSS network, the ETS and its role are defined and illustrated. Next, the matter of sensor selection for the ETS is discussed. This is followed by the consideration of the problem of point-source detection. A semi-empirical model which indicates the point-source detection capabilities of the background-limited ETS electro-optical sensors is presented. Short discussions of the satellite population and the problems associated with the passive detection of space objects by reflected sunlight are followed by conclusions based upon brightness measurements made at the ETS during approximately two years of operation.

INTRODUCTION

Very soon after the launch of Sputnik I in 1957, the Air Force placed into operation fast-scanning radar systems and Baker-Nunn cameras to detect man-made objects in space. It became apparent in the next decade that none of the operational systems was adequate to keep pace with the growing satellite population. Smaller and smaller objects were being placed in increasingly distant orbits. With few exceptions, the radar systems possessed insufficient range or resolution to satisfy surveillance requirements. The optical/photographic techniques suffered from insufficient sensitivity and speed; that is, they were distinctly non-real time.

Early in the 1970's, motivated by the developing silicon diode array technology and the growing mini-computer technology, Lincoln Laboratory investigated the possibility of designing a nearly real-time, passive (i.e., reflected sunlight as the signal source), ground-based electro-optical system which would meet the major requirements for satellite surveillance: adequate point-source detection capability and large fields-of-view. This latter requirement and the new technologies served as the raisons d'etre for this investigation since several observatories had been observing satellites for years, but with small fields of view and only when given accurate pointing information.

A design, based on field data, for a low-cost system that would serve as a test-bed for the concepts and the sub-systems that might

be conceivably used in an "all-up" GEODSS (Ground Electro-Optical Detection and Space Surveillance) system was accepted by the Air Force in 1974. In September of 1975, an experimental test site (ETS) was placed in operation near Socorro, New Mexico, in the White Sands Missile Range. The experience gained at the ETS has given the Air Force a proof-of-concept data-base that will allow the Electronic Systems Division (ESD) to deploy, with confidence in their operational capabilities, GEODSS sites around the world.

THE GEODSS SYSTEM

The GEODSS system is to consist of several electro-optical sites located with approximately equal spacing around the globe to provide overlapping sky coverage. Under ideal conditions, no objects of interest will escape detection within a reasonable operating time. Each site is to perform a variety of search, track, metric, and photometric tasks on objects out to and beyond synchronous distances. The five major missions are: 1) Initial detection and track, 2) Detection and track of maneuvered objects, 3) Routine catalog maintenance, 4) Collection of brightness and signature data, and 5) Special classified tasks. The most important data set consists of the topocentric angular position of each object and the time of observation. These sets of data will form a vital data base not only for the GEODSS system but also for twenty-four hour, high-power radars performing special tasks. The significance of this is apparent when it is realized that the availability of a given ground-based electro-optical site is generally less than 30 percent primarily because of the requirement of site darkness and the need for reasonable atmospheric conditions.

THE EXPERIMENTAL TEST SITE (ETS) AND ITS OPERATION

As mentioned above, the ETS has served as a test facility for more than two years. Telescopes, detectors, displays, signal processors, detector aids, automatic satellite detectors, data processing techniques, and operational methods have either been evaluated, refined, or developed. These tasks have been performed by Lincoln personnel and by personnel of the Aerospace Defense Command assigned to the ETS. During their commission, a great deal of information has been learned about the characteristics of a good fraction of the deep-space satellite population. This information will be outlined after discussions of the ETS system, the detection problem, and the performance of the selected ETS sensor.

Figure 1 is an external view of the ETS looking in a south-easterly direction. Figure 2 shows, diagrammatically, the basic ETS system. Since the ETS is duplex, this figure represents one-half of the system. Two telescopes, in a 24' astronomical dome, are co-mounted on a polar-axis astronomical mount as shown in Figure 3. The main telescope is a 31", f/5, f/2.8 Ritchey-Chretien unit, providing nominal 1° and 2° linear fields of view on a flat 80mm faceplate located in the focal plane. The auxiliary telescope is a 14" f/1.7 folded Schmidt unit, providing a nominal 7° field of view on an 80mm faceplate. Operations are controlled from the console, as presented in Figure 4. A typical operational sequence will serve to indicate some of the capabilities of the

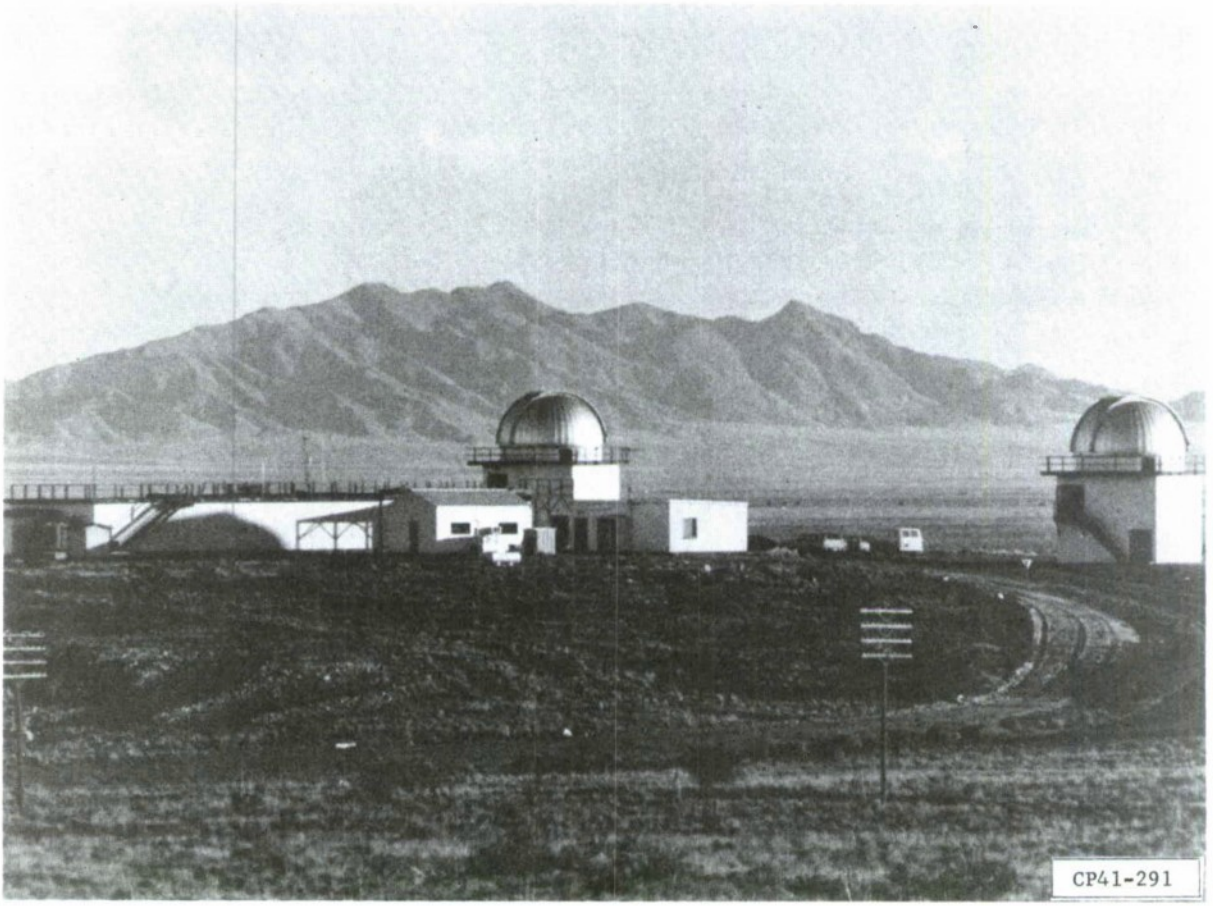

Fig. 1. External view of the ETS.

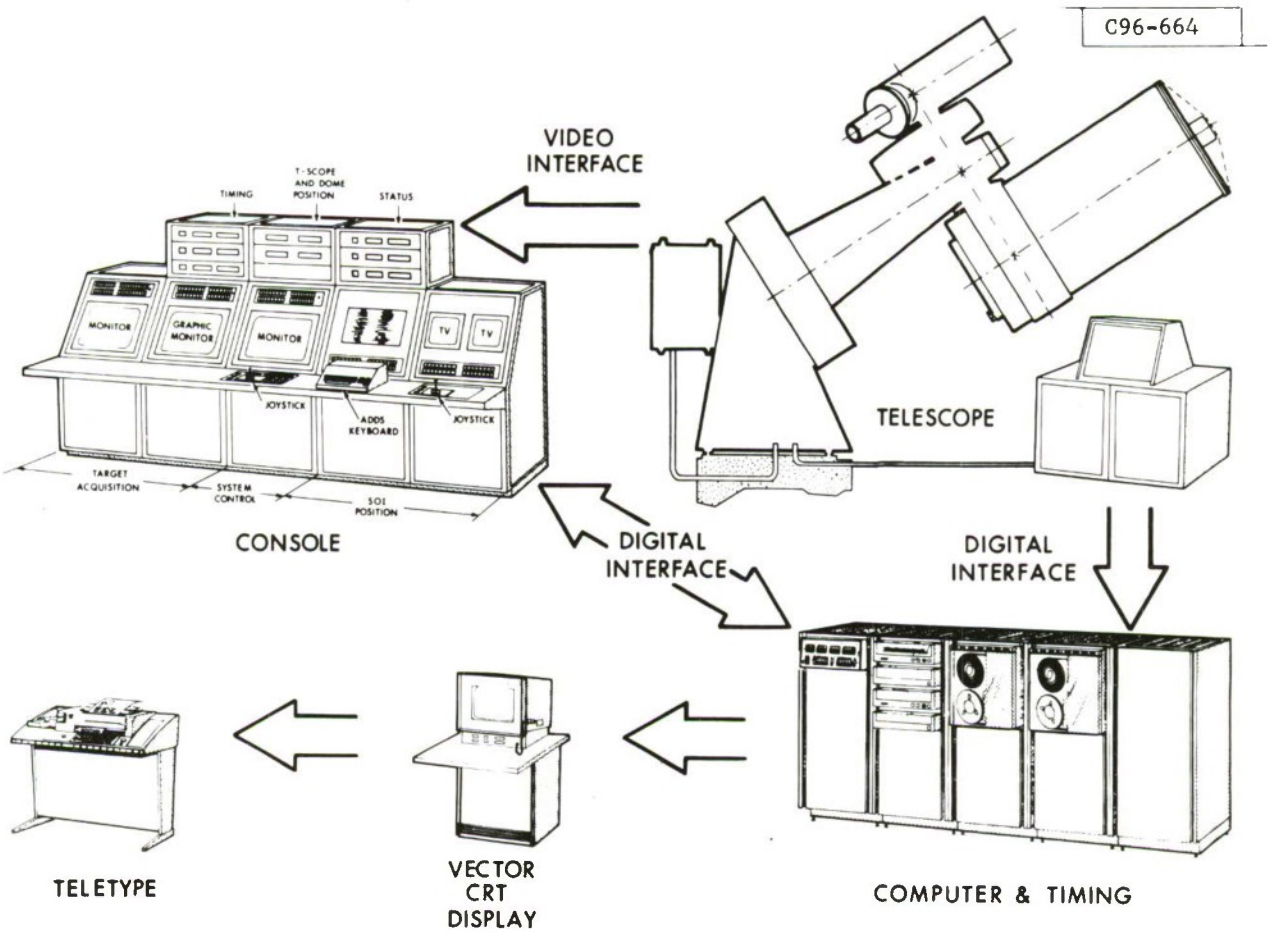

Fig. 2. Basic ETS configuration.

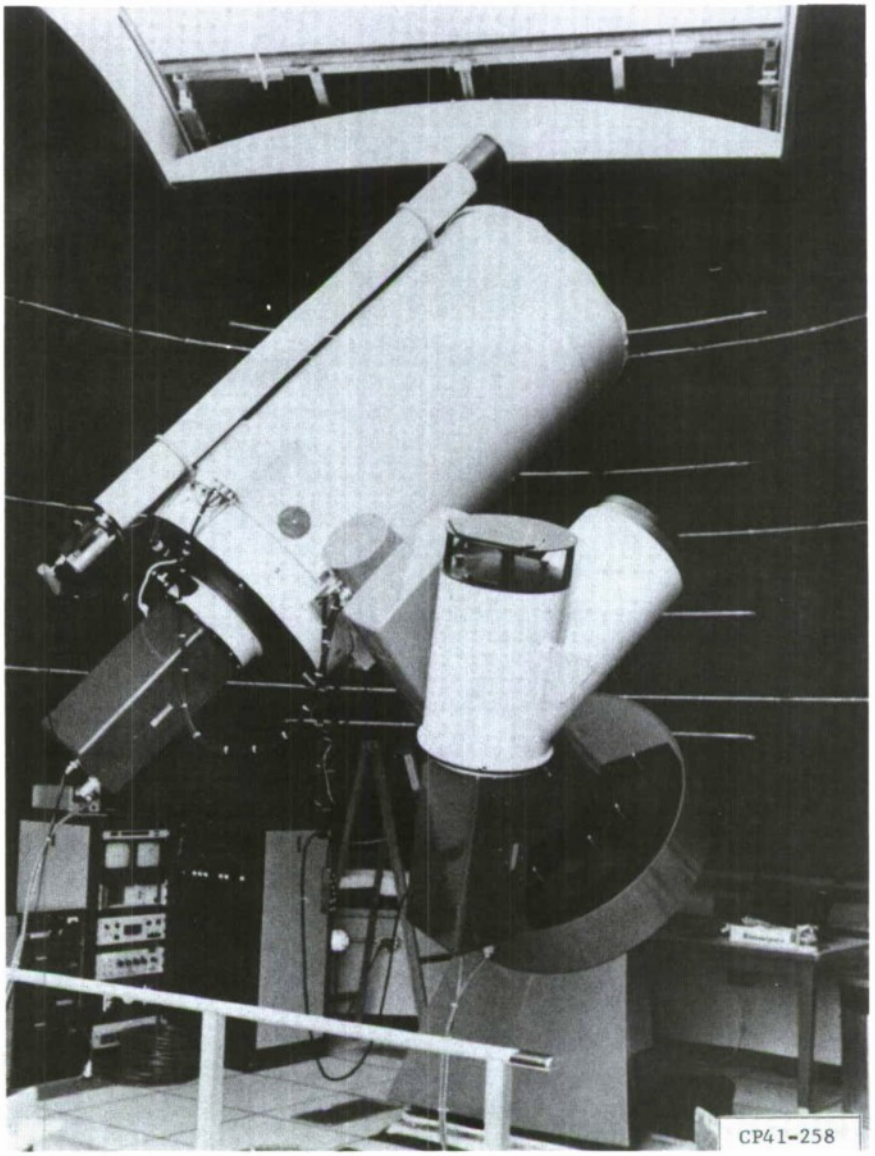

Fig. 3. Co-mounted ETS telescopes.

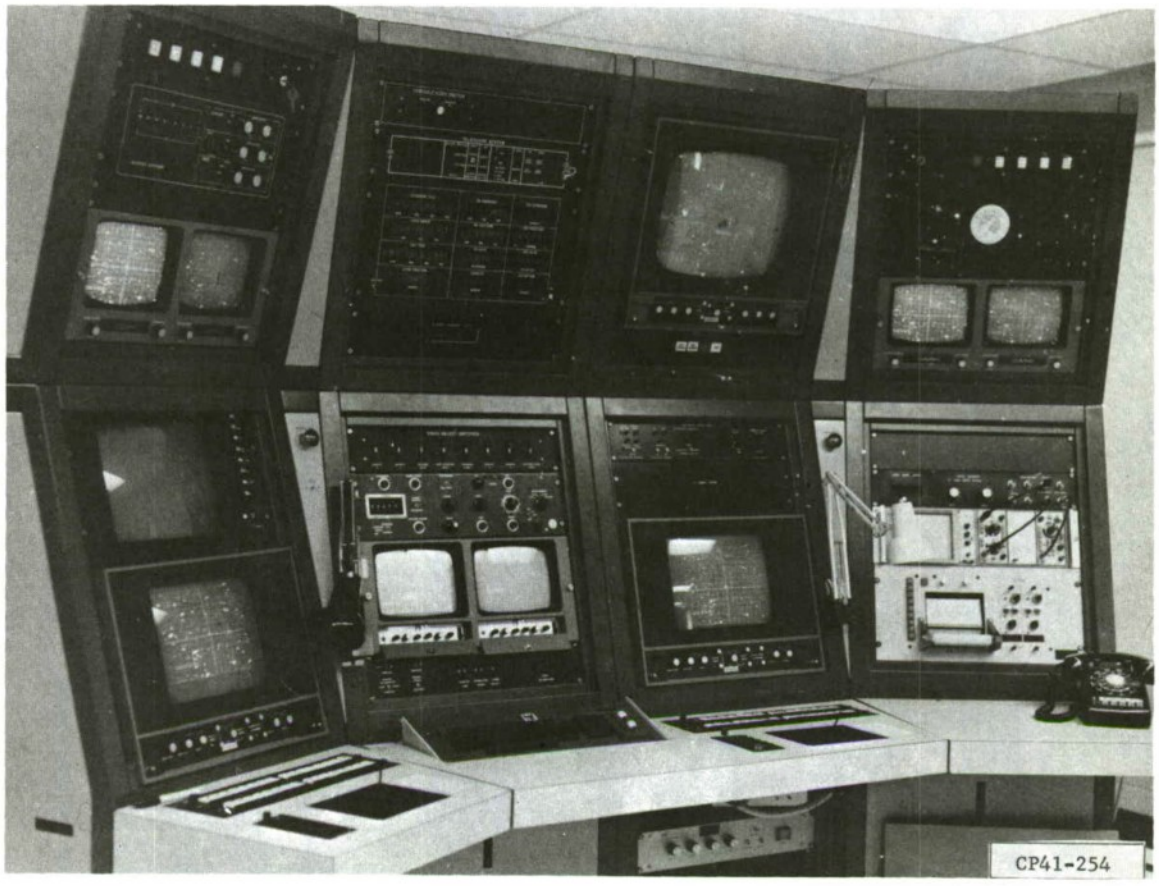

Fig. 4. ETS control console.

system. After twilight, with all systems in a state of readiness, the operator requests a calibration star in the vicinity of the anticipated detection and/or search, from the stored star file. The star is boresighted and the shaft encoders corrected. Then, by the use of pre-programmed buttons, the operator may request measurements of the brightness of the night sky (NSB) and of the atmospheric extinction coefficient[1] in the neighborhood of the anticipated satellite detection. The collection of these data requires approximately fifteen minutes. Then a satellite is requested by number from the satellite file. The telescope slews to the predicted position and the sidereal rate is resumed. If detected, the satellite is boresighted and the time and position recorded by the press of a button. For increased metric accuracy, electronic zoom may be used and additional calibration stars may be called from the stored SAO catalog. If desired, the object can be automatically tracked from its ephemeris and the offsets from its predicted track recorded for a period of time. While in track, the signal strength may be recorded either directly from the video signal or by the use of a GaAs photometer[2]. Then, for the purposes of comparative photometry, the signal strengths of known G-type stars[3,4,5] in the vicinity, as well as NSB signals, are recorded as appropriate. If signature data are of interest, the telescope is returned to track and an amplitude-time curve is recorded either on an analogue chart or stored digitally in the

computer. If the satellite is not detected in the initial field of view, several search routines may be called up. Upon detection of an object during search, a program is called into play which displays on the graphic terminal the locations of all satellites on file within a specified number of square degrees. This procedure reduces the occurrence of erroneous detections. It should be noted that if it is planned to look at a number of satellites during the observing session, a dynamic scheduler program[6] can provide a schedule which "catches" the satellites at their best weighted (priority, brightness, and closeness to the present field of view considered) times.

In view of the above, it is clear that the computer plays a critical role in the semi-automatic operation of the system. The present computer is a MODCOMP IV-25 which provides 256 kilobytes of core and includes 25 megabytes of disc memory. The satellite file (containing ≈400 deep-space-object element sets) and the SAO file[7] (containing 250,000 stars) are the major files to which the computer has fast access.

MOVING TARGET INDICATOR SYSTEMS AND INTEGRATION

There are two areas where some of the real-time advantages of standard television rates have been sacrificed. The first is in the development of moving target indicator (MTI) devices and the second is in the use of integration techniques (on the target of the camera tube and in external units) to gain extra detection capability.

Two MTI devices have been approved for possible use at GEODSS sites. The first[8] is a semi-automatic device which was designed and developed by Lincoln Laboratory for use as an operator aid. The heart of the system is an analog video disc recorder. The recorder simultaneously records and plays back the incoming video signal, providing a channel with a delay of up to four seconds with respect to the incoming video. This delayed channel is subtracted from the incoming video and all apparently stationary objects (i.e., stars) are removed. The satellite which has moved with respect to the stationary field is not subtracted.

In addition to the subtraction process, there are 14 fixed track heads arranged in groups of eight and six to provide up to 48 frames of integration. In the normal mode of operation, the integration is performed after subtraction to enhance the signal to noise ratio before detection.

After differencing and integration, the signal is sent to a constant false alarm rate (CFAR) detector which sets a threshold

such that an average of 200 detections per frame is maintained. The detections on successive frames are stored in scratch-pad memories and a comparison is made to determine a spatial correlation between detections. If there is a detection on a given location for a majority of successive frames, i.e., 2 of 3, or 3 of 5, or 4 of 7, a detection is registered and a cursor is put on the screen to indicate that location.

A variety of displays is possible. The subtracted result with cursor is one possibility. Figure 5 shows the unsubtracted display with cursors around three Molniya satellites in the same field of view. Figure 6 is a one minute photographic integration of the paths of the objects of Figure 5. The almost sub-liminal false-alarm cursors do not bother the operator. This device has proved to be very effective in the detection of slow-moving, relatively faint objects in crowded star fields. Unfortunately, its detection sensitivity is approximately 3 1/2 times less than that of the "unaided" operator once the object is located. There is currently under development a delayed-time-integration technique which promises to ameliorate this situation.

The second MTI system is an automatic MTI (AMTI) system[9,10]. This system was developed for the Air Force primarily by TRW Systems, Incorporated, with an assist from the ITEK Corporation. TRW developed the software (called ASTROSO) while ITEK developed the preprocessor. As in the video disc MTI system, the streak

Fig. 5. Video disc MTI display.

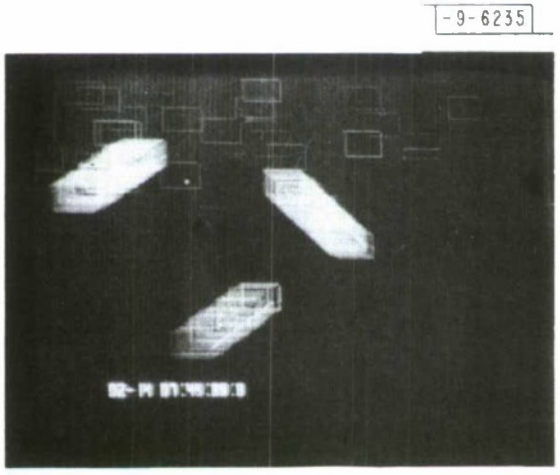

Fig. 6. Time exposure of video disc MTI display.

made by an object as it traverses the field of view provides the basis for detection in the TRW AMTI system.

The video image frames are thresholded into a binary format in the preprocessor. The computing requirements are determined by the field of view (fov) and the size of an image cell. At each sidereal fov, a set of six image frames is stored. One of these frames has a longer exposure time than the others so that it may be used for background rejection. The first "link" of ASTROSO builds a composite frame and rejects stationary background images (the so-called "OR-frame"). The next link prioritizes the image data and locates streak segments. The last link connects streak segments caused by the same object and detects false alarms. The visual outputs of the system are a processed frame and a printout of the results of the three software links. Internally, the angular velocity vector of the object is available. This will assist in the identification of the detected object. Figure 7 shows the frame when two Russian Molniya satellites were detected in the same field of view. Figure 8 shows the printout for the frame of Figure 7. Under Streak Data, the negative-two indicates that the software has ruled out the noise bursts on the lower edge of the frame as threats. The nine columns contain position and decision information used to verify the threats. The cycle time per fov is approximately five seconds for synchronous objects in a linear fov of 1^{o} with the present sensors. The TRW AMTI

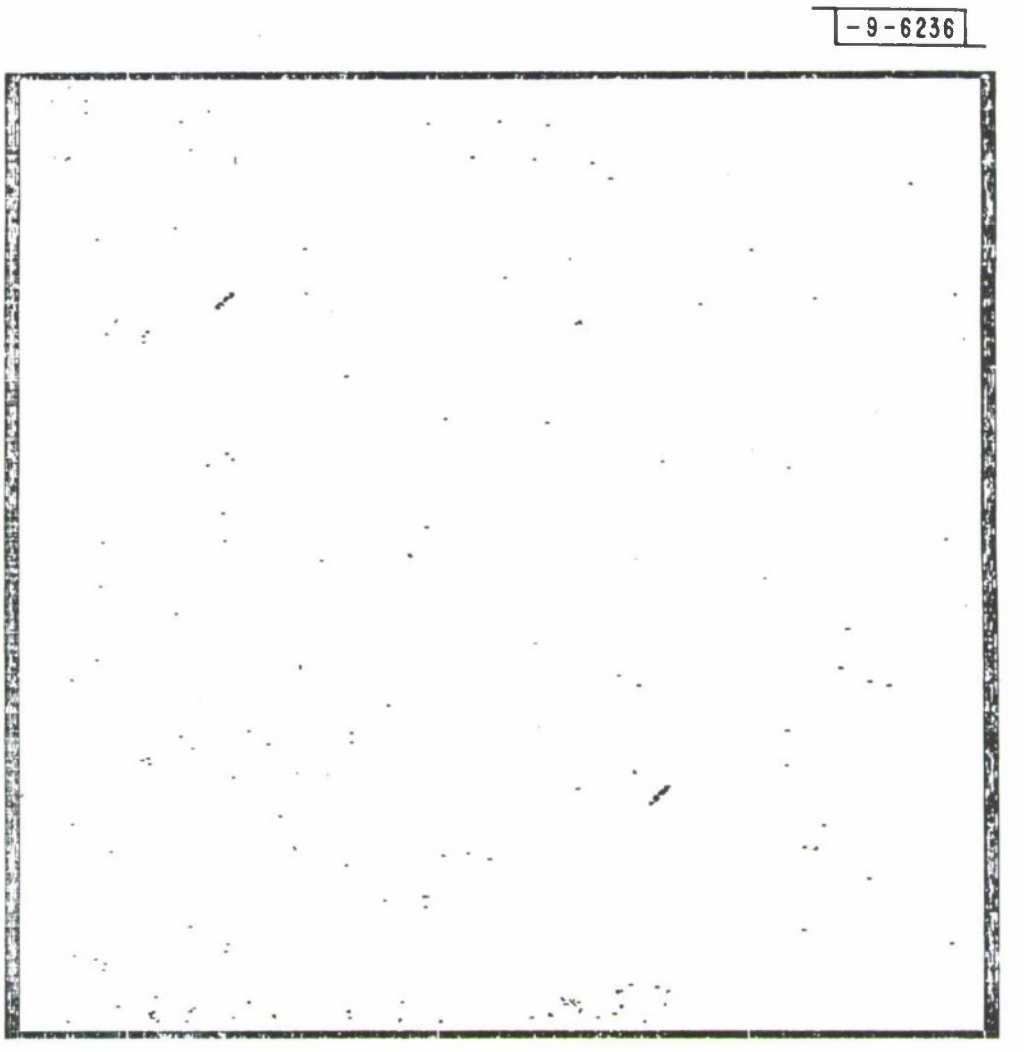

Fig. 7. AMTI processed frame.

```
$REW DSC TEM
$ASS 11 TEM 8 CSW 9 BSW
$REW 8 9 11
$NOTE        MGR PROCESSING STARTING   8:03:13
$EXE L2MGV2.XX


    THE CP TIME FOR LINK II MGR"IS      0.285SECONDS
$NOTE        MGR PROCESSING FINISHED   8:03:15
$WEO 8
$REW 8
$NOTE    LINK II PROCESSING STARTING   8:03:16
$EXE L2HUGH.XX
PROCESSED ALL LSC ENTRIES


    THE CP TIME USGD BY DRIVE IS      2.085SECONDS
$NOTE    LINK II PROCESSING FINISHED   8:03:22
$WEO 9
$REW 9
$NOTE   LINK III PROCESSING STARTING   8:03:22
$EXE L3V3CH.XX
```

****THREAT DATA****

STREAK DATA

1	2	3	4	5	6	7	8	9	THREAT NO.
109.960	98.400	25.0	-0.8252	13.010	0.150	0.187	0.569	0.0	1
364.276	322.172	29.0	-0.8092	13.518	0.135	0.180	0.532	0.0	2
NO THREAT STREAKS									
474.000	81.400	5.0	-0.8598	4.555	0.263	0.253	0.865	0.0	3 -2

```
    THE CP TIME FOR LINK III      0.465
    THE ELAPSED CLOCK TIME IS     0.880
$NOTE   LINK III PROCESSING FINISHED   8:03:26
$REW LO
```

Fig. 8. AMTI decision factors.

system performed well during its evaluation at the ETS. For static signal-to-noise ratios of six, the probability of detection exceeded 0.95 with less than one false alarm per twenty data sets. It was possible to discount false alarms quickly by operator intervention.

The need for integration on the target of the camera tube (possibly in combination with integration in an external analog terminal) arose because of the existence of a number of normally very faint man-made objects in space. This method is most useful when the object can be tracked, i.e., its ephemeris is known. By modest techniques, at room temperature, it has been possible to gain more than a factor of ten in detection sensitivity during track. Figure 9 indicates an integration detection in a moderately crowded star-field. The integrated image appears near the center of the field of view. This exposure was made in the Milky Way.

Fig. 9. Integration in tracking mode.

SENSOR SELECTION FOR ETS

Astronomers and land-based satellite observers have at least one common problem: How to deal with the complex radiation pattern presented by a faint point-source image located between a celestial background and an atmospheric foreground. Of course, the point source image at the aperture is not a point, but a disc whose diameter is determined primarily by atmospheric turbulence. The angular diameter of this seeing disc averages about two arc-sec at a good site. After a series of field tests in 1972, it was decided that low-light-level, beam-scanned, television camera tubes of the intensified silicon-diode array type, generically called Ebsicons, possessed the potential capability of resolving the aforementioned radiation pattern into its spatial, temporal, and amplitude characteristics in approximately real-time. The real-time requirement reduced the number of choices from those available to astronomers. Ebsicons promised high sensitivity, adequate image cell size (i.e., each image cell would not collect an inordinate amount of background charge when coupled to a typical 30", f/5 telescope), moderate charge storage capability, useful dynamic range, acceptable saturation characteristics, a virtually burn-proof target, a rugged package, simple operation, and finally, high pre-scanning gain. The last characteristic suggested the possibility of operation in the photon-noise-limited regime under dark skies. This mode of operation is such that the total

instrument noise per image cell when referred to the first photocathode, for example, is negligible compared to the statistical noise generated in the conversion of signal and background optical flux into photoelectron signal and background counts at the surface. For a given electro-optical sensor, once this regime is reached, the basic limitations imposed by the laws of probability must be accepted. In the present situation, where the exposure time is limited, the largest affordable aperture and the highest available quantum efficiency of the first photocathode are desirable for optimum detection capability. No amplification process after the first photosurface can compensate for not having used the largest aperture and the highest quantum efficiency. If the condition of real-time (1/30 second) is relaxed, since a linear increase in background counts does not require the same linear increase in signal counts to maintain a constant coefficient of performance, the limit of detection improves with exposure time as long as the storage capability of the detector has not been reached and it is no longer determined by either the aperture or the quantum efficiency.

The early field tests indicated the usefulness of an external, single-stage, image converter (IC) tube coupled to the Ebsicon[11]. On the same telescope, under identical conditions, using the same Ebsicon, a single IC increased the point source detection capability by a factor of six on typical observing evenings.

Another important advantage was realized by the use of a 2:1 demagnifying IC. For a given telescope, the areal fov was increased by a factor of four. This is important in surveillance. This also meant that in the design of a future system, lower cost telescopes (higher f/number) could be specified. Finally, the increased pre-scan electron gain (≃25) provided by the external converter, allowed the use of uncooled, 7.5mHz video preamplifiers under the darkest of skies at ETS. Under the present mode of operation, predominantly at television rates, the advantages of an external stage of amplification outweigh the disadvantages: increased image cell size, increased shading, increased number of ionic scintillations, decreased effective storage capacity, increased complexity, increased size and weight, and increased cost. It is to be noted that as soon as large-format Ebsicon tubes (80mm input photocathode)[12] with high pre-scan gain (≃4000) become available, especially if the real-time requirement is relaxed, the need for an external converter stage will no longer exist for electro-optical sensors with typical apertures of one meter and linear fov's of the order of 2^{o} in the present application.

In accordance with the decision to employ intensified Ebsicon assemblies, ETS experimental/operational cameras were specified by Lincoln and constructed by Westinghouse. The cameras use Varian VL-116 (80/40) image stages and Westinghouse WX-32719

(40/32 or 25) Ebsicon camera tubes. The "32 or 25" refers to the diameter (in mm) of the DEMC silicon diode array targets. The Ebsicons containing the 32mm targets were developed for ESD by Westinghouse (tube fabrication) and Texas Instruments (target fabrication) under the management of the Night Vision Laboratory. The program is presently under Lincoln management. Figure 10 shows a 40/32 WX-32719 tube received under the contract.

The operation of the Ebsicon sensor may be described briefly as follows: Photons incident on the first photosurface are converted to photoelectrons which are accelerated to the back-biased diode array (the target). Each photoelectron releases approximately 2,000 electron-hole pairs in the silicon on which the array has been fabricated. The holes are swept to the p-sides of the diodes, reducing the back-bias potential. The current which flows as the read beam (electrons) restores the bias potential to its initial values constitutes the video signal. In the original procurement for the ETS-cameras, S-20 photosurfaces and P-20 phosphors were specified. At the present time, improved surfaces may be available[13].

Under the tube/target research and development contract mentioned above, large-format deep etched metal capped (DEMC) targets[14] were developed. Their geometry improves the beam-acceptance and blooming performance as compared to conventional resistive sea and metal pad targets. While the promised

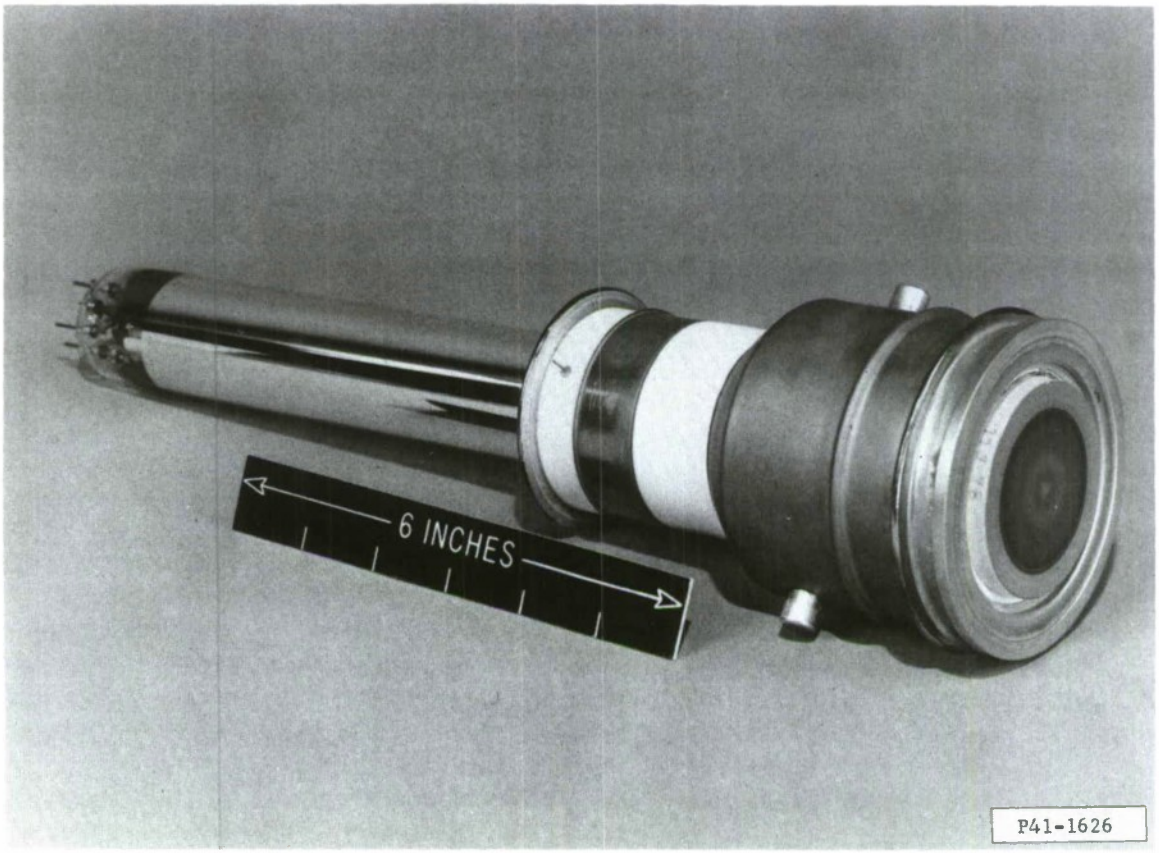

Fig. 10. WX-32719 Ebsicon camera tube.

improvements have materialized, the presence of blemishes (especially white blemishes) has kept the yield of acceptable 32mm targets at a very low level.

THE PROBLEM OF POINT-SOURCE DETECTION

In an attempt to understand the detection of point-source signals, bare and intensified Ebsicons have been studied in the laboratory and in the field. The tests and results to be discussed here deal primarily with unintensified (bare) Ebsicons. Qualitatively, the results apply to the intensified case; quantitatively, the increase in image cell size must be accounted for in the intensified case. With tungsten radiation modified by an eye filter to approximate reflected sunlight, a series of spots of differing diameters, d, were focused onto the faceplate of the camera operating in its most sensitive mode. With a video line passing through the peak of the video response, and far from saturation [15], the full linewidth at 0.50 amplitude (FWHA) was measured. Figure 11 presents the resulting plot of d versus FWHA. It is seen that for $d \simeq 30\mu$ a factor proportional to the effective image resolving power of the total camera system has been reached. This is fortunate in the sense that the 31", $1^{o}.16$ ETS telescope provides a point image approximately of diameter 25μ (i.e., ≈80 percent of light included) for G-type point sources on a good night. The effective image cell diameter at the output, d_o, of the camera may be calculated from the expression $d_o = d_h t_f / t_h$, where d_h is the scanned horizontal length on the target, in microns; t_f is the FWHA, μsec; and, t_h is the effective horizontal scan time, in μsec. In the 4 x 3

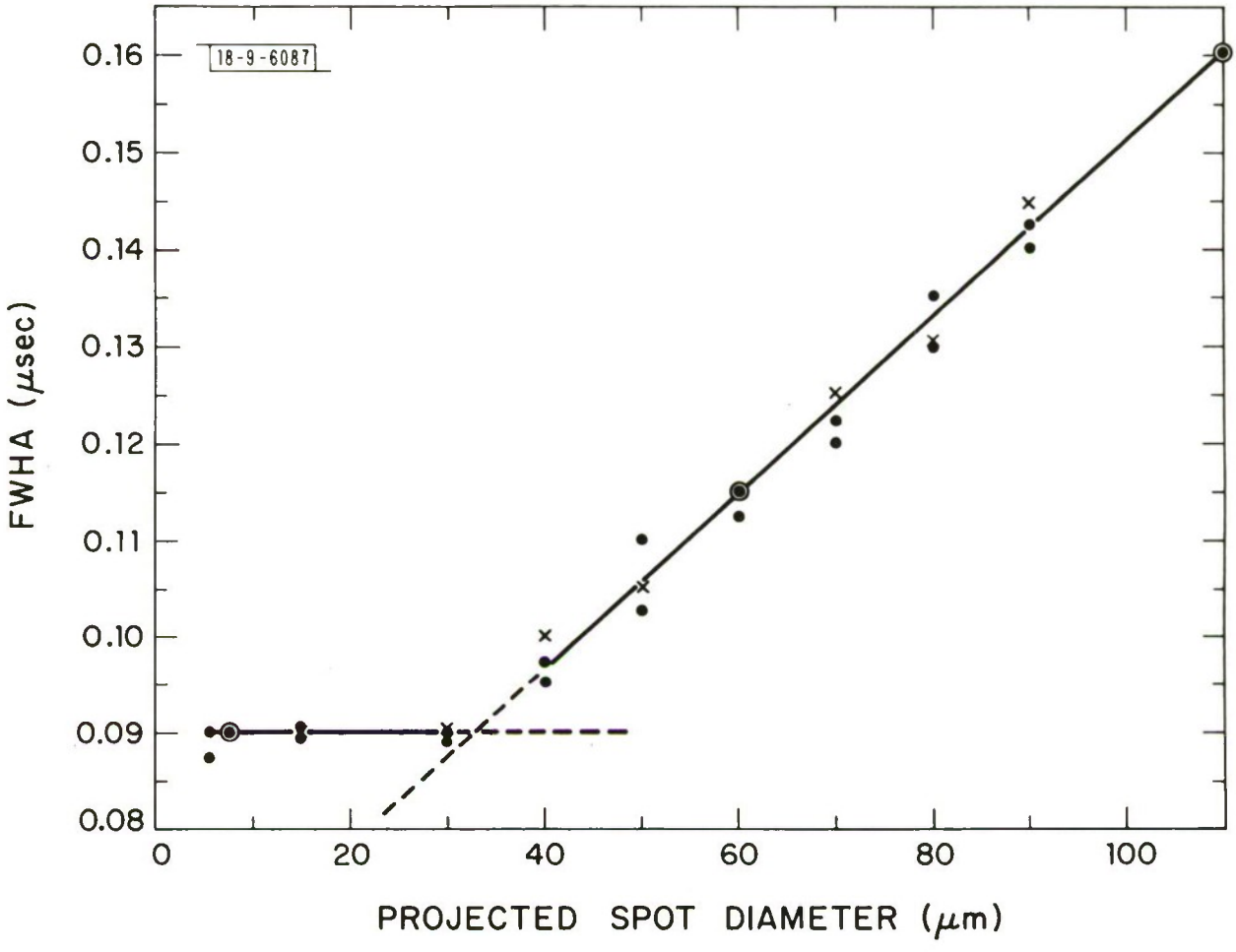

Fig. 11. Point-source video linewidth vs projected spot diameter.

television format, $d_h = (32.)\ (.8)\ 10^3$ and $t_h = 54.0$ μsec. Then, for $t_f = 0.090$ μsec, $d_o = 42.7$ microns.

Next, two point sources, each of diameter 30μ on the face-place, were projected onto the same horizontal line and were made to move towards each other as the modulation (the dip between peaks/amplitude) and the "distance" between peaks were recorded[16]. The results are presented in Figure 12. In this experiment $t_f = 0.100$ μsec and corresponded to 2.25 of the arbitrary units used in the figure. At 0.50 modulation, the separation between peaks was 1/0.30 = 3.33 units, or 0.148 μsec; while for 0.10 modulation, the separation was 0.10 modulation, the separation was 0.125 μsec. This gives a measure of the point-source resolving capability.

Attention was then paid to the shape of the point-source distribution as viewed on the screen of an A-scope. Using the standard 30μ spot with a scan line through the peak, line shapes were carefully measured for t_f's ranging from 0.080 to 0.120 μsec. Standard deviation values were read off from the 0.61 response points and each curve was compared to an appropriate Gaussian distribution. Without exception, the fits were excellent down to the 0.3 response point. For lower responses, the Gaussian fit fell slightly below the observed values (i.e., the Gaussian fits had shorter tails). For example, with an observed response of 0.08, the Gaussian fits varied between responses of 0.05 to 0.07.

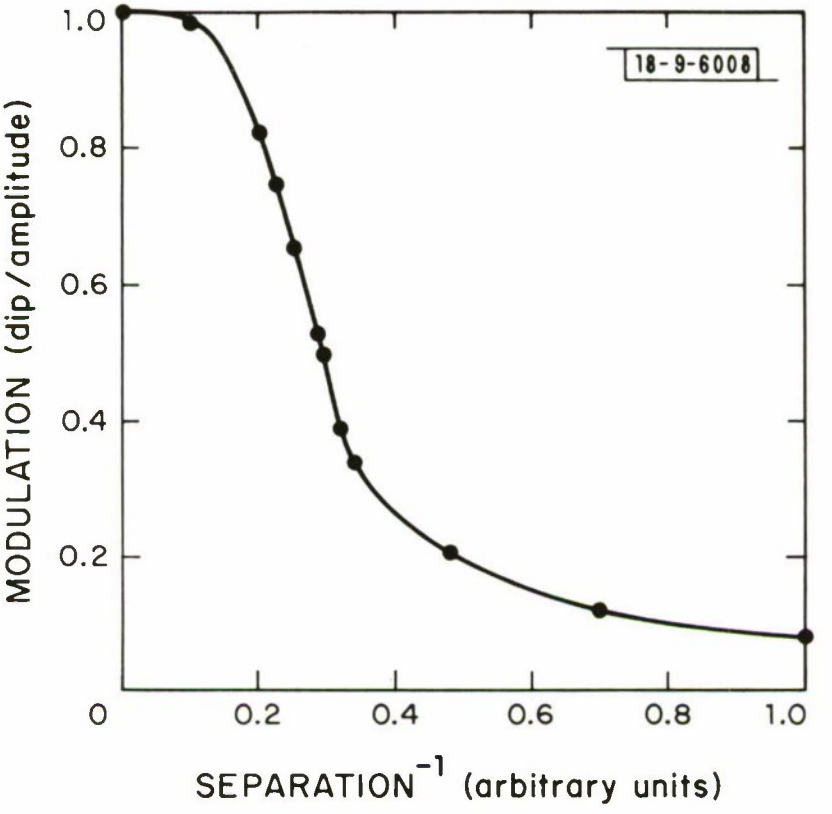

Fig. 12. Modulation vs separation of two point-sources.

Intuitively, it is not surprising that the point response of the system is very nearly Gaussian in nature. The signal photons pass through the telescope, pass through the fiber optic faceplate, and are finally converted to photoelectrons (a Poisson type process). These particles pass through the electron optics, interact with the silicon lattice to produce new information charge which is then read out by a profiled electron beam. That charge then flows through a resistor to be observed as a voltage on the A-scope. The central-limit theorem appears to be alive and well.

Analyses have indicated that if the point source response is very nearly Gaussian in nature, the sine wave response (and the square wave amplitude response) may be calculated directly from a single, careful measurement of t_f. Thus far, with t_f between 0.080 and 0.140 μsec, the calculated square wave amplitude response values have agreed well with the measured values as taken with an RCA P-200 test chart. Figure 13 shows a plot of t_f versus the expected (calculated) square wave amplitude response (SWAR) at the 0.50 point in TVL/Raster Height (19.2m). This is convenient to use once it is known that the total point source response of the system is approximately Gaussian in nature. As soon as more data are collected, the details of this calculation and method, if they continue to be experimentally verified, will be presented in a detailed paper.

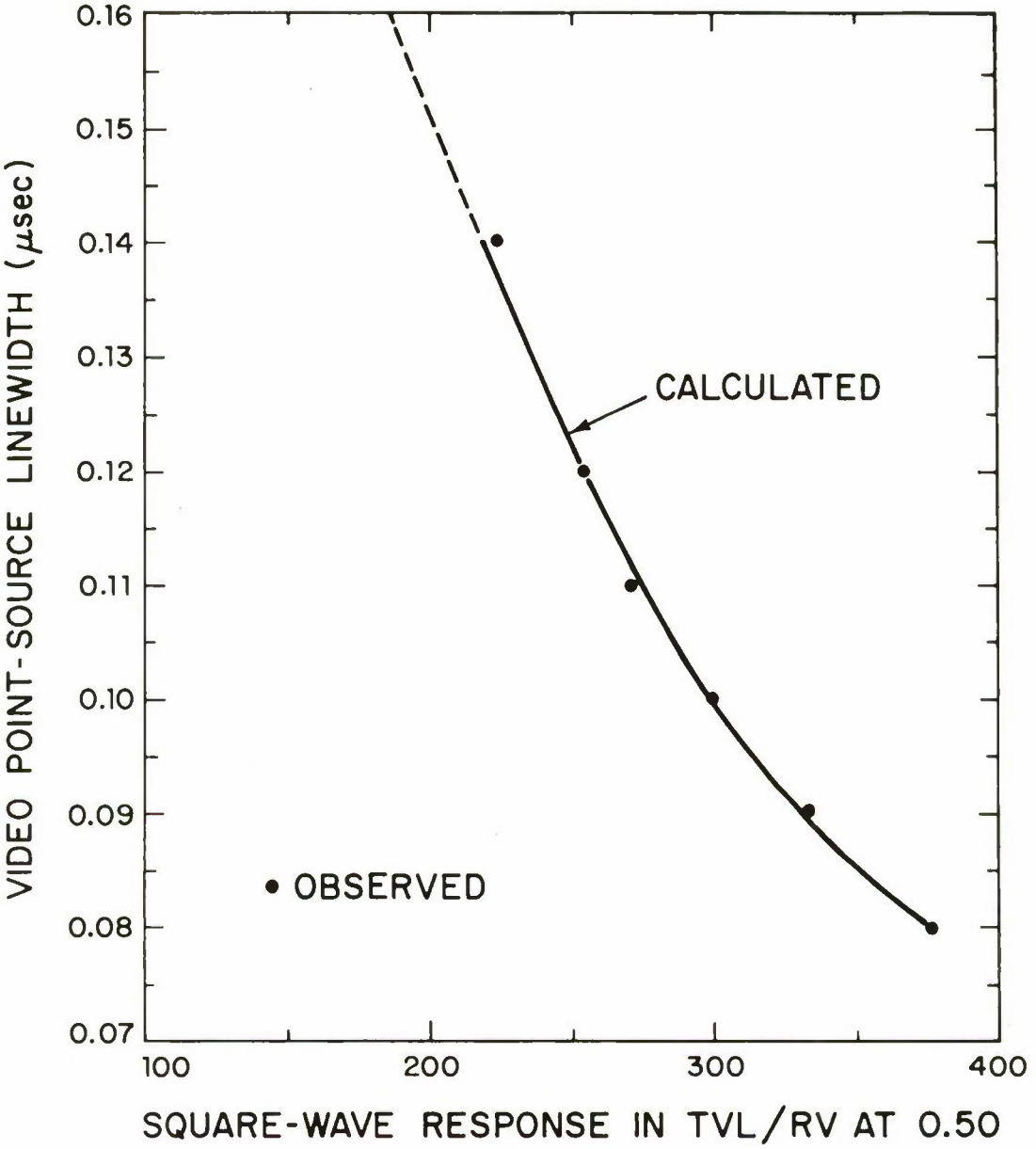

Fig. 13. Point-source video linewidth vs 0.50 square response.

A SEMI-EMPIRICAL SENSOR MODEL

In developing an empirical model for the detection capability of the ETS sensors, instrument noise, dark current noise, and all other camera noise sources may be justifiably neglected due to the high pre-scan electron gain of the system. The geometric image cell diameter, α, is taken to be t_f converted to arc-sec through the expression α = fov (degrees, diagonal) (3600) (0.8) $t_f t_h^{-1}$. Thus, for the intensified Ebsicon case, where t_f is typically 0.120 μsec and for the 31", 1°.16 ETS telescope, α = 7.4 arc-sec.

The point-signal photoelectrons in an image cell at the first photosurface are given by $S = s\pi D^2 \eta t/4$[11], where s† is the number of photons/m^2/sec from the point source, at the aperture; D is the 100 percent transmission, zero obscuration, diameter of the aperture in meters; η is the broadband quantum efficiency of the first photosurface to the incident photons; and t is the exposure time (1/30 second for TV rates). The number of background photoelectrons in an image cell at the first photosurface is given by $B = b\pi D^2 \eta t \alpha^2/4$, where b† is the background photon rate in m^{-2} arc-sec^{-2} at the aperture, and α is the diameter of the image cell in arc-sec. It has been found that a good approximation to the video signal-to-noise ratio (SNR_V), as determined by dividing the mean peak signal voltage by the adjacent rms noise voltage, is given by

---

†s and b are average values.

$$(SNR)_V = k \frac{S}{(B)^{1/2}} = k \frac{sD}{2\alpha} \left(\frac{\pi\eta t}{b}\right)^{1/2}, \qquad (1)$$

where k is an empirically determined number, determined to be 3/4 in the steady state operation of the sensor. This number takes into account certain system losses and gains. For example, a single scan line through the signal peak does not sense all of the positive charge in an image cell on the target for at least two reasons; in addition, the effective background sampling area appears to be less than the effective signal sampling area.

Detailed calculations have related s and b† to visual magnitudes referenced to our sun with zero air mass[17]. Figure 14 indicates the result. A word about visual magnitudes: the brightness response of the eye is logarithmic. A change in brightness of 2.512 times corresponds to a change of one visual magnitude - a change of 100, to five "vismags". The brighter the source, the smaller its absolute numerical vismag. This is a carry-over from the astronomers of old. In this system, our sun's vismag is approximately $-26^m.8$. A properly illuminated sphere of $1m^2$ cross-section and 0.1 reflectivity placed in synchronous orbit would appear as a $15^m.5$ star in the heavens to a ground-based observer.

Returning to the use of Figure 14 and Eq. (1). For the ETS 31", $1^o.16$ telescope, D ≃ 0.5m, α = 7.4 arc-sec, and η = 0.072. $(SNR)_V$ becomes $2.2 \times 10^{-3} s/(b)^{1/2}$. For a 21^m sky (dark) and a

†b is appropriate for moon-lit skies.

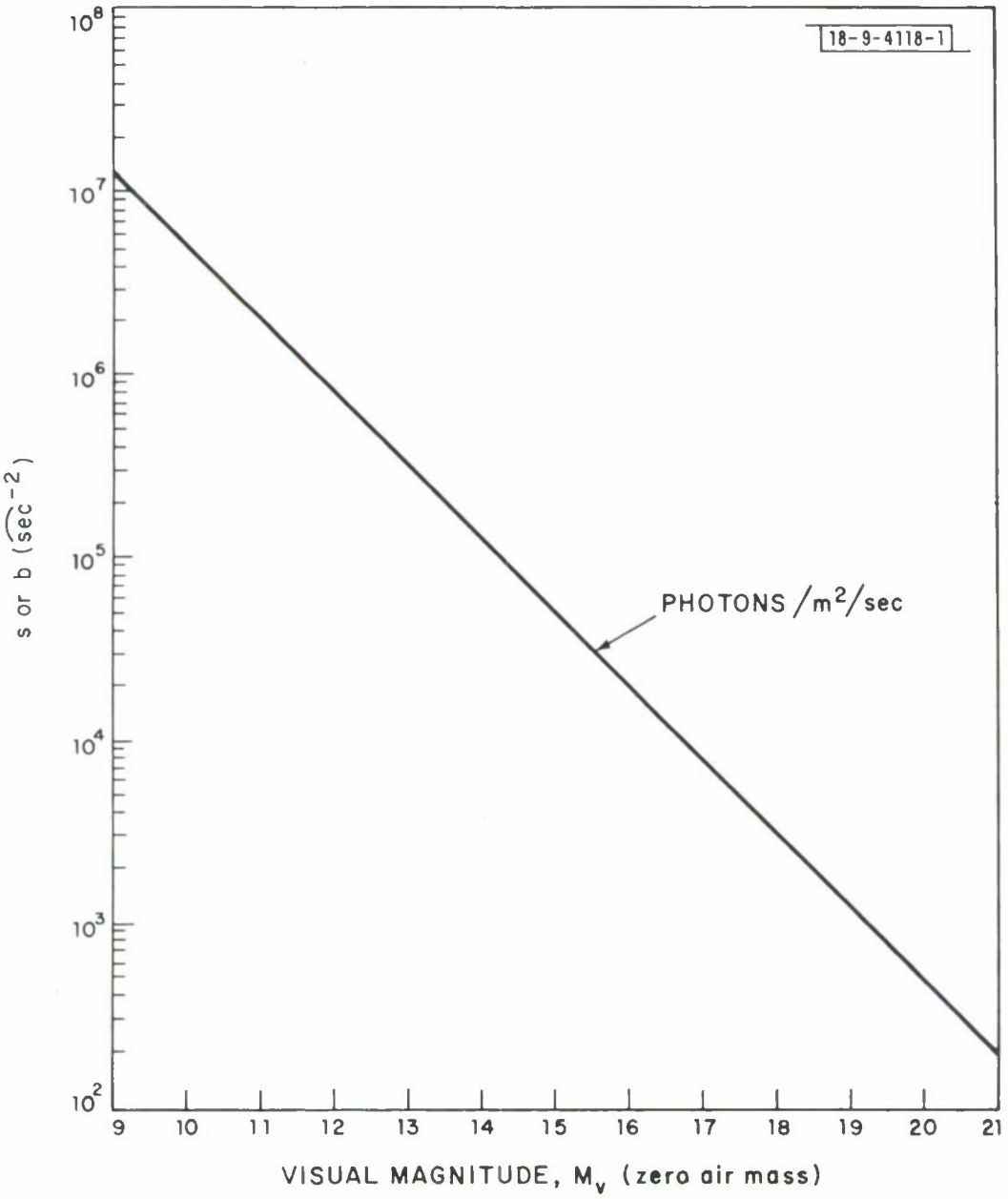

Fig. 14. Signal and background flux densities vs magnitude.

17^m object (faint), $(SNR)_V \simeq (2.2 \times 10^{-3})\ (8 \times 10^3)/(200)^{1/2}$ $\simeq 1.2$. This object would be visible on the face of a video monitor. If the total atmospheric extinction is accounted for ($0^m.2$ - $0^m.5$ at the ETS), the detectivity would be reduced accordingly to objects between $16^m.8$ and $16^m.5$. The correctness of Eq. (1) has been verified at the ETS for typical sky brightnesses and for linear fov's ranging from approximately $0^o.5$ (zoom) to 7^o (auxiliary telescope). Eq. (1) appears to be somewhat optimistic for skies brighter than 19^m, possibly because of scattered light in the telescope and sensor.

In the development of Eq. (1), sky brightnesses and atmospheric extinction coefficients were measured photometrically. Point source vismags were determined by comparative means using carefully selected G-type calibration stars. The maximum errors in the measurements were ten percent.

DWELL-IN-THE-CELL MODE OF OPERATION

In MTI schemes operating in the sidereal mode it is sometimes advantageous to integrate for a dwell-in-the-cell time, t_d[11]. For example, a synchronous object moving at an apparent angular speed, ω, of 15 arc-sec/sec with respect to the stars, spends approximately 0.5 second in a geometric image cell. Thus, approximately 15 times the 1/30 second exposure at TV rates is available for integration. In general, $t_d = \alpha c/\omega_d$, where $c \simeq 0.8$ reflects the fact that the dynamic dwell-cell is effectively smaller than the geometric cell[10]. Here, the signal and beam shapes and relative motion are coming into play. By substituting $\alpha = \omega_d t_d/c$ into Eq. (1), Eq. (2) results:

$$(SNR)_v = \frac{kc}{2} \frac{s}{(b)^{1/2}} \frac{D}{\omega_d} \left(\frac{\pi\eta}{t_d}\right)^{1/2} \qquad (2)$$

Since $t_d \propto \alpha$, it is clear that for a given sky brightness, a given camera, and a required $(SNR)_v$, the minimum detectable signal $s \propto \alpha^{1/2}\omega_d{}^{1/2}D^{-1}$. For a given value of D, then, a four-fold improvement in α would be as effective as increasing D by a factor of two while maintaining the original α-value.

It is to be noted that once a system is adjusted for a specific ω_d-value, the $(SNR)_v$ as given by Eq. (2) for objects faster than ω_d is decreased by the ratio of ω_d to ω. This is a reflection of that fact that for $\omega > \omega_d$, less signal charge is deposited in an image cell for a given value of t_d.

For the same conditions as in the previous example (ETS 31", $1^{o}.16$ telescope; $\eta = 0.072$; $D \simeq 0.5m$, 21^{m} sky) but with a system tuned to $\omega_d = 15$ arc-sec/sec ($t_d = 0.4$ sec), with slow read out, and with the requirement that $(SNR)_v = 1.2$ for visibility on the monitor, s is calculated from Eq. (2) to be 2.34×10^3 photons/m^2/sec. From Figure 14, this corresponds to a point source signal of magnitude 18.4 at the aperture.

OBSERVED CHARACTERISTICS OF THE SATELLITE POPULATION

The majority of the space objects (payloads, rocket bodies, and pieces of debris) of primary interest to ETS are located in orbits with ranges between 3,000 nmi and 20,000 nmi. The apparent angular speeds vary from approximately six arc-sec/sec to 300 arc-sec/sec. The characteristic dimensions cover an interval of from one to thirty meters. The main structures may be of any shape, many contain booms, and may be stabilized or not. A few typical shapes are presented in Figure 15. Active payloads are generally stabilized while inactive payloads, rocket bodies, and pieces of debris tumble in orbit. The payloads may be covered with solar cells, or may contain paddles which contain solar cells. The sun-illuminated areas of differing reflectivities visible from the darkened site at any instant of time determine the detection radiation pattern. The amplitude versus time history of this pattern constitutes the signature data upon which space object identification (SOI) depends. An historical signature file, or base, is most useful in detecting changes in stabilization or in detecting shape differences in a given family of objects. Figure 16 shows the signature trace of an object with a spin period of approximately ten sec. Four rotating solar-cell booms provided the interesting structure.

There are probably between 400 and 500 space objects within the coverage of the ETS. Perhaps 25 percent of these are in

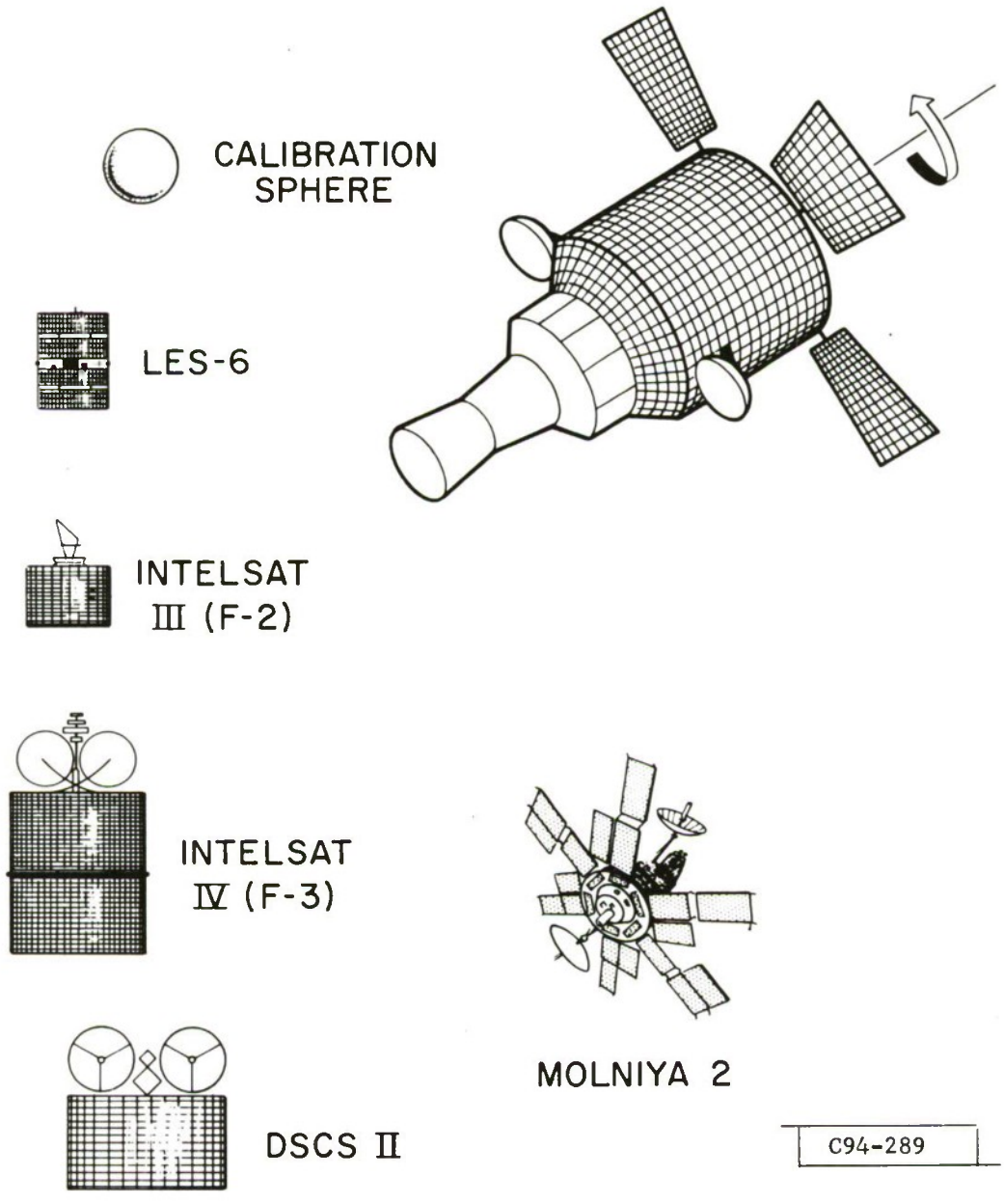

Fig. 15. Some interesting space objects.

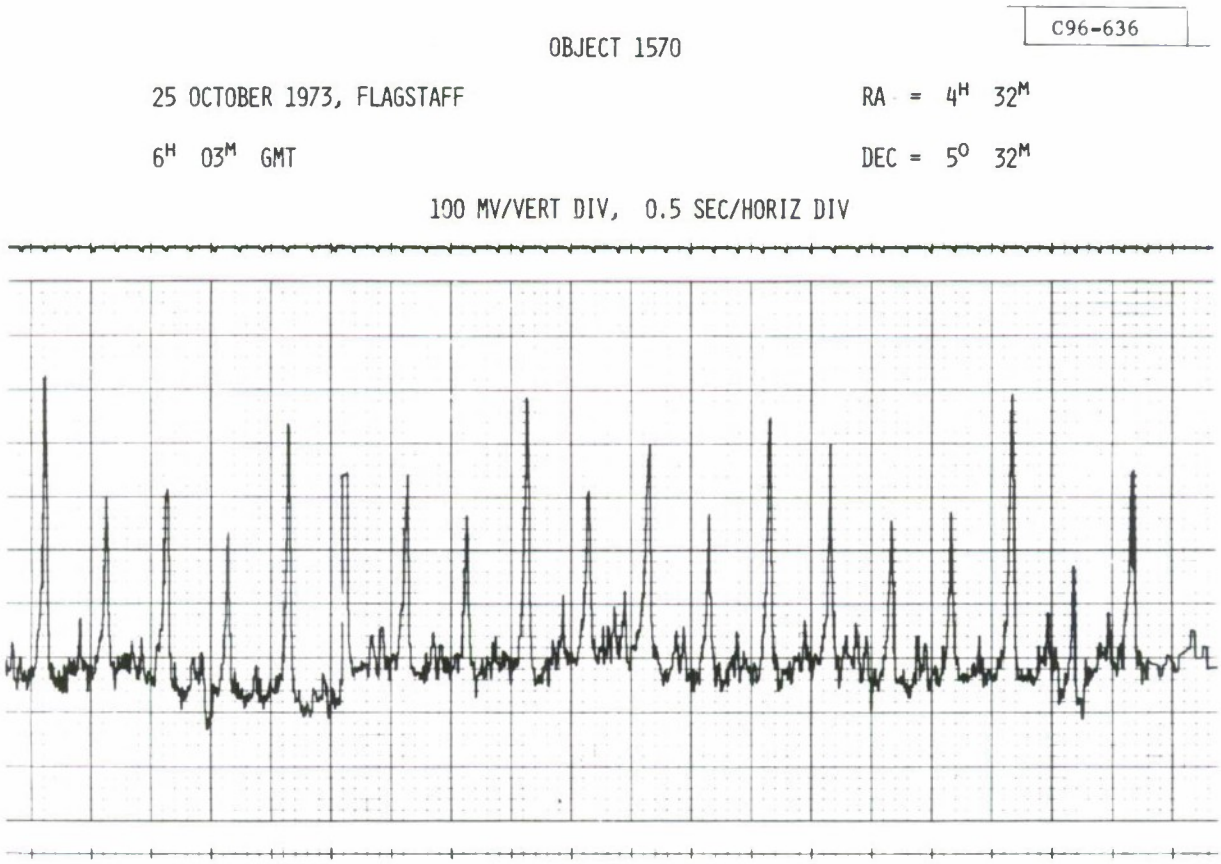

Fig. 16. Amplitude vs time recording.

nearly circular equatorial orbits with periods of approximately 24 hours. A like number are in twelve-hour elliptical orbits with apogees in the North. The majority of the former objects "belong" to western countries, while the majority of the latter belong to the Soviet Union. The latter payloads pass over North America and the Soviet Union every 24 hours. These are the Molniya communications satellites. The remaining objects possess apogee distances which range from hundreds of miles from the surface of the earth to approximately 100,000 miles. Given sufficient time, all space objects except for a few geo-synchronous vehicles are viewable from a site such as the ETS.

Payloads are of primary interest. To aid in the identification of new payloads, a catalog of space objects must also contain detailed information about rocket bodies and pieces of debris. In catalog maintenance, where the position of a known object is to be checked, the most important satellite characteristic in so far as successful detection is concerned is the brightness-time history of that object. Given acceptable atmospheric conditions, a schedule may be made, based on that history, which insures its detection. This is true for all orbits.

The measurements of approximately 40 different synchronous payloads indicate that the average diffuse brightnesses vary down to about $16^{m}.5$ with a peak in the distribution near $15^{m}.5$. This is important information to have in the case of a search for a new,

a lost, or a maneuvered synchronous satellite. The dwell-in-cell technique for $\omega_d \simeq 15$ arc-sec/sec may be used to excellent advantage in a search of this type.

Observations in the Molniya belt along the ETS orbital extremes indicate that the diffuse brightnesses range from $9^m.5$ to $15^m.5$. The apogee brightness distribution peaks at approximately $14^m.3$. Once again, for the detection of a known object, its brightness-time history assures its detection. However, a search for an unknown satellite in the belt is complicated since the speed of the object changes with time. During an observing period, the speed may vary from hundreds of arc-sec/sec to approximately six arc-sec/sec. Since the faster objects are brighter, it may be advantageous to search in the dwell-in-cell mode with the device "tuned-up" for the lower speed. The loss of charge in an image cell due to the excessive speed (>6 arc-sec/sec) is compensated for by the increased brightness.

The problem of an arbitrary, fast, all-sky search in an AMTI mode of operation for uncatalogued space objects will not be discussed in this paper. The wide range of speeds (~6 to 300 arc-sec/sec) and brightnesses to be anticipated indicate that several systems may be necessary. For example, the fact that approximately one-half of the deep space population appears to consist of objects brighter than $14^m.5$ may be used to define a division of the task among the electro-optical systems involved in the search.

A few words about scan coverage rate (SCR) are appropriate at this point. In a cost-effective system, the maximum diameter of the telescope, because of a telescope/mount cost breakpoint, is approximately one meter. The maximum acceptable linear fields of view (fov) provided in the focal plane by reasonable optical designs may be calculated by use of the specified diameter of the first photocathode of the accepted low-light-level camera system. Knowing the number of linear point-source image cells provided by the camera system, a typical exposure time for a given satellite speed and for each considered fov may be determined from an anticipated processing scheme. This exposure time, in conjunction with the required limiting detection capability of the system under specific observational conditions, allows the determination of the actual detection capability of the electro-optical system for each linear fov. Should this capability be deficient, the fov must be decreased (the f-number increased) until the desired result is realized. Once realized, the total time spent in each fov (processing plus moving and settling times) is known. Thus, the maximum SCR at the required detection threshold is determined. If this SCR is insufficient, an additional system may be required; if excessive, fov may be traded for increased detection capability (or D reduced). The important point is that the required detection capability under the specified observational conditions and the exposure time calculated from the processing scheme determine the maximum possible SCR.

The ETS results presented thus far have dealt with diffuse scattering from the space objects. In the diffuse-scattering regime, Lambertian scattering models are useful. Near the equinoxes, specular returns[18] from the objects may be observed. Whenever the angle of incidence of the sunlight with respect to the reflecting surface is equal to the angle between the normal at the point of incidence and the observer, all in the sun-satellite-site plane, a specular return occurs. This return may be many times stronger than the diffuse return. For example, the specular return for a $1.0m^2$ plate with a reflectivity of 0.10, at synchronous distances, would be visible to the naked eye of an observer on the ground.

In order to detect and define the orbits of satellites which are usually below the detection threshold of the ETS system (approximately 20 percent of the deep-space population), it has been desirable to anticipate the times when it may be possible to observe specular reflections from these satellites. An analysis of this timing for cylindrical, spin stabilized (i.e., spin axis parallel to the axis of the earth) satellites has resulted in a computerized prediction generator[19]. Since the Lambertian model of diffuse reflection is frequently inadequate near specular occurrence, empirical curves have been developed from experimental data to provide more reliable brightness models.

A time exposure of the specular returns from the satellite LES-6 is shown in Figure 17. This satellite's spin-symmetry axis misalignment is primarily responsible for its complicated return.

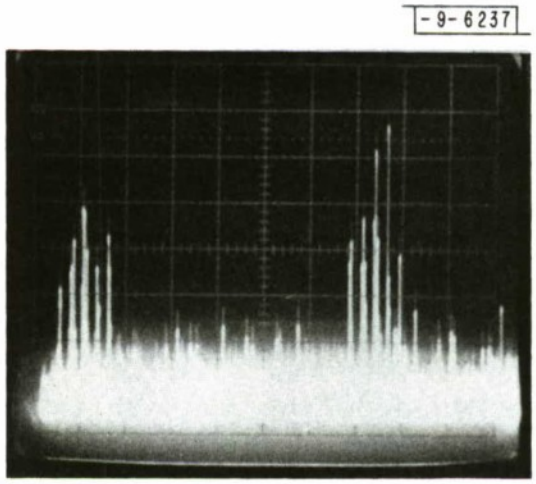

Fig. 17. Time exposure of specular returns from LES-6.

CONCLUSION

The role of the ETS in the GEODSS program has been defined. The choice of sensor, the problem of point-source detection, and a model which describes sensor performance at the ETS have been described. Observations of the characteristics of the satellite population - all performed with the intensified Ebsicon systems - have been presented. It is expected that the ETS (perhaps in modified form) will continue in operation within the GEODSS system as an evaluation facility for electro-optical sensors and signal processors and as a training site for Air Force personnel. We look to the future for improved camera systems. Within the next decade it should be possible to replace beam-scanned GEODSS camera systems with low-noise, efficient, solid-state devices. These devices will bring us closer to the realization of an ideal detector. In addition to their obvious advantages, their low noise, increased quantum efficiency, increased dynamic range, reduced lag, improved geometric fidelity, and superior metricity should satisfy the detector requirements for the efficient detection and surveillance of satellites for years to come, either from the ground or from space.

ACKNOWLEDGMENTS

The author wishes to thank his colleagues at Lincoln Laboratory and at the ETS for their varied contributions to this paper. He is particularly indebted to Dr. E. Rork for many of the satellite brightness measurements. Finally, the skillful typing of the manuscript by P. L. McDonald is acknowledged.

REFERENCES

1. J. M. Sorvari and C. E. Beane, "Automatic Real-Time Extinction Measurement," Project Report ETS-17, Lincoln Laboratory, M.I.T. (12 September 1977), DDC AD-A046484/2.

2. R. Weber, "The Detection Capabilities of Gallium Arsenide and S-20 Photo-Multiplier Tubes to GO-Type, Point-Source, Signals," Technical Note 1976-13, Lincoln Laboratory, M.I.T. (3 March 1976), DDC AD-A023818/8.

3. A. U. Landolt, Astron. J., 78, No. 9, 959 (1973).

4. A. Th. Purgathofer, "UBV Sequences in Selected Star Field," Lowell Observatory Bulletin No. 147, Vol. VII, No. 10 (22 January 1969).

5. O. J. Eggen and A. Sandage, Astrophys. J., 158, 669 (1969).

6. W. J. Taylor, "A Dynamic Satellite Scheduling Algorithm," Project Report ETS-15, Lincoln Laboratory, M.I.T. (7July 1977), DDC AD-A043636/0.

7. L. G. Taff, "The Handling and Uses of the SAO Catalog," Project Report ETS-6, Lincoln Laboratory, M.I.T. (5 November 1976), DDC AD-A035871/3.

8. G. T. Flynn, "An Electro Optical MTI System for the Detection of Artificial Satellites (the NITH Finder)," Technical Note 1977-32, Lincoln Laboratory, M.I.T. (27 June 1977), DDC AD-A048055/8.

9. "Laboratory and Field Testing of the Realtime Streak MTI Process," TRW Final Report (January 1977).

10. R. Weber, "Field-Testing and Evaluation of the TRW Streak MTI System," Project Report ETS-13, Lincoln Laboratory, M.I.T. (9 June 1977), DDC AD-B020022-L.

11. R. Weber and T. H. Brooks, "The Limits of Detectability of a Low-Light-Level Point-Source Sensor as a Function of Telescope Aperture, Sensor Resolution, Night-Sky Background, and Pre-readout Electron Gain," Technical Note 1974-21, Lincoln Laboratory, M.I.T. (16 August 1974), DDC AD-785137/1.

12. V. J. Santilli and G. B. Conger III, Adv. Electron. Electron Phys. 33A, 219 (1972).

13. R. Weber, "Photoemissive and Electroemissive Surfaces and Sandwiches," Technical Note 1977-18, Lincoln Laboratory, M.I.T. (25 May 1977), DDC AD-A042431/7.

14. M. Green, A. B. Laponsky, and W. D. Frobenius, "EBS Tubes with Deep-Etch Metal-Cap Targets," presented at Electro Optical Systems Conf., Stuttgart (October 1973).

15. R. Weber, "The Amplitude Effect of Point-Source Blooming as a function of Background Level in Ebsicon-Type Camera Tubes," Technical Note 1977-31, Lincoln Laboratory, M.I.T. (16 June 1977), DDC AD-A043277/3.

16. "Determination of Infrared Camera Tube Characteristics," Report of the Working Panel, published in Proc. IRIS 10, 49 (1966).

17. R. Weber, "Visual Magnitude Flux Rate Density Standards for Sunlight Incident on Photoemissive Surfaces," Technical Note 1974-20, Lincoln Laboratory, M.I.T. (6 May 1974), DDC AD-779822/6.

18. A. S. Friedman, "Determination of Specular Reflection from Cylindrical Satellites for Electro-Optical Surveillance and SOI," Project Report ETS-3, Lincoln Laboratory, M.I.T. (8 October 1976), DDC AD-A034580/1.

19. A. S. Friedman, "Wide Band Optical Observation of Cylindrical Geostationary Satellites," Proc. Ninth Annual NORAD Spacecraft Identification Conf., Colorado Springs, 26-29 July 1977.

UNCLASSIFIED

SECURITY CLASSIFICATION OF THIS PAGE *(When Data Entered)*

REPORT DOCUMENTATION PAGE		READ INSTRUCTIONS BEFORE COMPLETING FORM
1. REPORT NUMBER ESD-TR-78-213	2. GOVT ACCESSION NO.	3. RECIPIENT'S CATALOG NUMBER
4. TITLE *(and Subtitle)* The Passive, Ground-Based, Electro-Optical Detection of Synchronous Satellites		5. TYPE OF REPORT & PERIOD COVERED Technical Note 6. PERFORMING ORG. REPORT NUMBER Technical Note 1978-27
7. AUTHOR*(s)* Robert Weber		8. CONTRACT OR GRANT NUMBER*(s)* F19628-78-C-0002
9. PERFORMING ORGANIZATION NAME AND ADDRESS Lincoln Laboratory, M.I.T. P.O. Box 73 Lexington, MA 02173		10. PROGRAM ELEMENT, PROJECT, TASK AREA & WORK UNIT NUMBERS Program Element No. 63428F Project No. 2128
11. CONTROLLING OFFICE NAME AND ADDRESS Air Force Systems Command, USAF Andrews AFB Washington, DC 20331		12. REPORT DATE 19 June 1978 13. NUMBER OF PAGES 54
14. MONITORING AGENCY NAME & ADDRESS *(if different from Controlling Office)* Electronic Systems Division Hanscom AFB Bedford, MA 01731		15. SECURITY CLASS. *(of this report)* Unclassified 15a. DECLASSIFICATION DOWNGRADING SCHEDULE

16. DISTRIBUTION STATEMENT *(of this Report)*

Approved for public release; distribution unlimited.

17. DISTRIBUTION STATEMENT *(of the abstract entered in Block 20, if different from Report)*

18. SUPPLEMENTARY NOTES

None

19. KEY WORDS *(Continue on reverse side if necessary and identify by block number)*

GEODSS	satellite detection	point source detection
Experimental Test Site	passive detectors	satellite population

20. ABSTRACT *(Continue on reverse side if necessary and identify by block number)*

M.I.T. Lincoln Laboratory is engaged in supporting the Electronic Systems Division (ESD) of the Air Force Systems Command (AFSC) in developing the Ground-based Electro-Optical Deep Space Surveillance (GEODSS) system. As a part of this program an Experimental Test Site (ETS) has been established in the White Sands Missile Range, New Mexico, to serve as a test-bed for the system. After a brief description of the GEODSS network, the ETS and its role are defined and illustrated. Next, the matter of sensor selection for the ETS is discussed. This is followed by the consideration of the problem of point-source detection. A semi-empirical model which indicates the point-source detection capabilities of the background-limited ETS electro-optical sensors is presented. Short discussions of the satellite population and the problems associated with the passive detection of space objects by reflected sunlight are followed by conclusions based upon brightness measurements made at the ETS during approximately two years of operation.

DD FORM 1 JAN 73 1473 EDITION OF 1 NOV 65 IS OBSOLETE

UNCLASSIFIED

SECURITY CLASSIFICATION OF THIS PAGE *(When Data Entered)*